Quasi-Static Magnetic-Field Technique for Determining Position and Orientation

FREDERICK H. RAAB, SENIOR MEMBER, IEEE

Abstract—**Multiaxis generation and sensing of magnetic-dipole fields is used to determine both position and orientation. The effect of conducting ground upon the fields is kept to an acceptably low level by using extremely low-frequency source-excitation signals. This technique can therefore be used in through-the-earth position-finding for applications such as drill guidance and mine rescue. The theory of operation, system-design procedures, and simulated performance data are given.**

I. Introduction

LOW-FREQUENCY quasi-static magnetic fields have been used in numerous short-range position-measurement, orientation-measurement, and guidance systems. Some techniques use fields generated by loops, while others use fields generated by long wires. Most of the techniques are based upon free-space quasi-static field geometry. Subsurface use of such systems requires the use of excitation frequencies low enough (e.g., 10 Hz) to reduce the effects of the conducting earth to an acceptably low level.

The position-finding technique employed by the present generation trapped-miner location system [1]-[3] requires physical movement of a receiver on the surface to locate a null in the vertical magnetic field produced by a buried magnetic dipole (loop-antenna transmitter). The buried dipole is assumed to be vertically oriented, hence deviations from true vertical orientation produce errors in the estimated position. Recently developed techniques [3]-[6] overcome this problem by measuring the magnetic field at three or more locations with three-axis sensors; the dipole location is determined by a series of iterative computations. Another recent approach [7] locates a single-axis subsurface antenna by retransmission (relay) of phase measurements made on dipole fields produced by transmitters on the surface. The SPASYN system [8] varies the excitation of its three-axis magnetic-dipole source to track the position of its three-axis magnetic sensor.

The system discussed here [9] uses both a three-axis magnetic-dipole source and a three-axis magnetic sensor, along with related electronic circuitry (Fig. 1). Optionally, either the source *or* the sensor (but not both) can have only two axes. The source axes are excited sequentially, at different frequencies, or in some other multiplexed format that allows separation of their signals by the receiver. Synchronization of the excitation and detection circuitry can be accomplished either by information contained in the transmissions or by information transmitted through another channel.

The computation and display circuitry and the sensing circuitry can either be colocated or connected by relay link. Position and orientation estimates are obtained through direct, closed-form computations that require no initial information and allow no "hang-ups." Since the source-excitation pattern is fixed, the positions and orientations of several receivers can be determined simultaneously.

One application of this system is the guidance of a remotely controlled underground drill, since both position and orientation measurements are required. Another application is the location of trapped mine workers; while only position information is required, degradation of position accuracy by an unknown antenna orientation is eliminated.

In both applications, a high-power two- or three-axis source is placed at a known location on the surface. Magnetic-field measurements made by the subsurface units are relayed to the surface for processing and estimation of position and orientation. For trapped-miner location, the beacon transmitter used in the present electromagnetic location system can provide the communications relay link.

This paper first establishes a coordinate frame and determines transformations that relate the source excitation to the sensor output. Equations for estimating position and orientation are then derived. Design considerations and procedures and simulated performance data are given.

II. Source-to-Sensor Coupling

This section defines the geometric parameters and presents the field-coupling relationships in matrix-equation form.

Geometry

The geometric relationship between the three-axis source and three-axis sensor is shown in Fig. 2. The *source coordinate frame* $X_1 - Y_1 - Z_1$ is defined by the axes of the source. Alignment of these axes with some convenient natural reference such as north, east, and down is assumed.

The sensor position is specified in rectangular (x, y, z) or spherical (α, β, ρ) coordinates defined relative to the source coordinate frame. Sensor orientation is specified by a sequence of three rotations (Euler angles). Azimuthal rotation by ψ first turns the sensor about its Z axis from $+X$ toward $+Y$. The elevation rotation by θ then turns the sensor about its Y axis from $+X$ to $-Z$. Finally, a roll rotation by ϕ turns the sensor about its X axis from $+Y$ to $-Z$. Note that in the zero-orientation condition, the three sensor axes are parallel

Manuscript received November 20, 1978, revised May 29, 1981.

The author is with Green Mountain Radio Research Company, 240 Staniford Road, Burlington, VT 05401. He was with Polhemus Navigation Sciences, a subsidiary of the Austin Company.

0196-9219/81/0010-0235$00.74

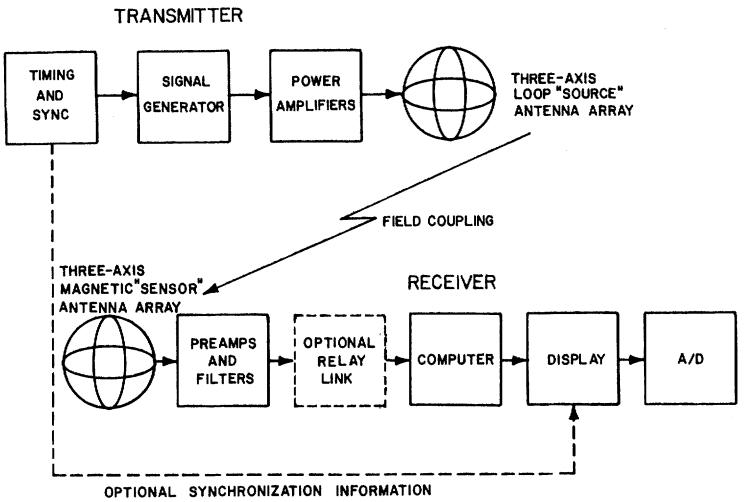

Fig. 1. Block diagram of magnetic-field-position-finding system.

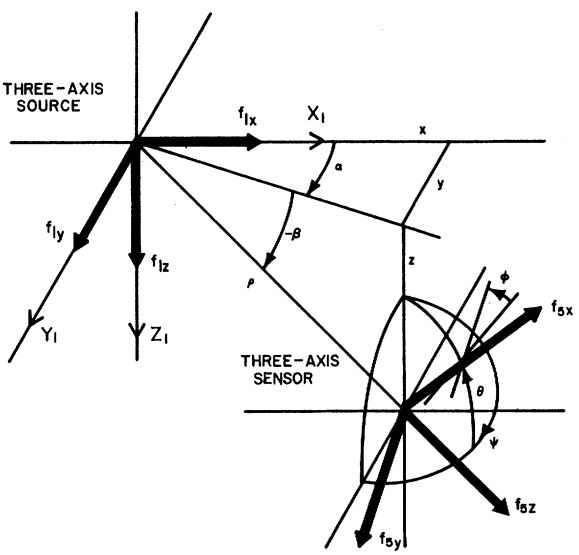

Fig. 2. Position and orientation coordinates.

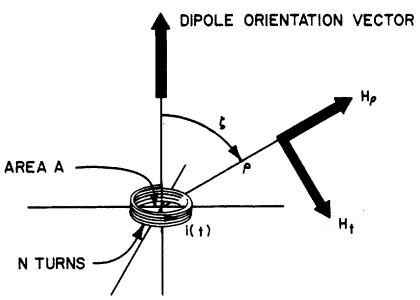

Fig. 3. Magnetic-dipole field components.

to the corresponding source axes, and that the order of the rotations cannot be interchanged without changing the value of ψ, θ, and ϕ.

Magnetic Dipole Fields

This system uses extremely low-frequency signals whose wavelengths are much greater than the distance separating the source and sensor. In addition, the diameters of the source and sensor loops are much smaller than the distance separating them. Under such conditions, excitation of the loop in Fig. 3 by a current $i(t) = I \cos \omega t$ produces the radial and tangential magnetic-field components [10]

$$H_\rho = \frac{M}{2\pi\rho^3} \cos \zeta \tag{1}$$

and

$$H_t = \frac{M}{4\pi\rho^3} \sin \zeta \tag{2}$$

where N, A, and $M = NIA$ are the number of turns, area, and *magnetic moment* of the loop, respectively. A temporal variation of exp $(j\omega t)$ is implied. Since the distance is much less than a wavelength, the phase shift of the signal between the source and sensor is negligible.

Matrix Representation of Source-Sensor Coupling

The excitation of a three-axis magnetic dipole source and the resultant three-axis sensor output are most conveniently described in vector notation. The excitation of the source is therefore represented by $\boldsymbol{f}_1 = [f_{1x}, f_{1y}, f_{1z}]^T$. The number of turns and area of the three source loops are assumed to be identical, hence f_{1x}, f_{1y}, and f_{1z} represent the amplitude of the currents exciting the loops of X-axis, Y-axis, and Z-axis orientation, respectively. The output of a three-axis sensor can be similarly represented by $\boldsymbol{f}_5 = [f_{5x}, f_{5y}, f_{5z}]^T$.

The source-to-sensor coupling equation can be derived conveniently [8] in matrix form by (1) rotating the source excitation vector by the position angles α and β to obtain radial and tangential components relative to the sensor location, (2) applying radial and tangential coupling relationship, (3) derotating the result into the source coordinate frame, and (4) rotating the result by the orientation angles. From [8],

$$\boldsymbol{f}_5 = \boldsymbol{R}\boldsymbol{f}_1 = \frac{C}{\rho^3} \boldsymbol{A}\boldsymbol{Q}\boldsymbol{f}_1 \tag{3}$$

where

$$\boldsymbol{A} = \boldsymbol{T}_\phi \boldsymbol{T}_\theta \boldsymbol{T}_\psi \tag{4}$$

TABLE I
ORTHOGONAL ROTATION MATRICES

	Position	Orientation
Azimuth rotates X into Y	$\boldsymbol{T}_\alpha = \begin{bmatrix} \cos\alpha & \sin\alpha & 0 \\ -\sin\alpha & \cos\alpha & 0 \\ 0 & 0 & 1 \end{bmatrix}$	$\boldsymbol{T}_\psi = \begin{bmatrix} \cos\psi & \sin\psi & 0 \\ -\sin\psi & \cos\psi & 0 \\ 0 & 0 & 1 \end{bmatrix}$
Elevation rotates X into $-Z$	$\boldsymbol{T}_\beta = \begin{bmatrix} \cos\beta & 0 & -\sin\beta \\ 0 & 1 & 0 \\ \sin\beta & 0 & \cos\beta \end{bmatrix}$	$\boldsymbol{T}_\theta = \begin{bmatrix} \cos\theta & 0 & -\sin\theta \\ 0 & 1 & 0 \\ \sin\theta & 0 & \cos\theta \end{bmatrix}$
Roll rotates Y into $-Z$	not applicable	$\boldsymbol{T}_\phi = \begin{bmatrix} 1 & 0 & 0 \\ 0 & \cos\phi & \sin\phi \\ 0 & -\sin\phi & \cos\phi \end{bmatrix}$

Inverses $\boldsymbol{T}_\alpha^{-1} = \boldsymbol{T}_{-\alpha}$, $(\boldsymbol{T}_\beta\,\boldsymbol{T}_\alpha)^{-1} = \boldsymbol{T}_{-\alpha}\,\boldsymbol{T}_{-\beta}$

is the orientation matrix (see Table I),

$$\boldsymbol{Q} = \boldsymbol{T}_{-\alpha}\boldsymbol{T}_{-\beta}\boldsymbol{S}\boldsymbol{T}_\beta\boldsymbol{T}_\alpha \tag{5}$$

includes the effects of the position angles (see Table I), and

$$\boldsymbol{S} = \begin{bmatrix} 1 & 0 & 0 \\ 0 & -\frac{1}{2} & 0 \\ 0 & 0 & -\frac{1}{2} \end{bmatrix} \tag{6}$$

represents radial and tangential coupling.

Excitation States

Determination of position and orientation requires sensor outputs corresponding to two or three linearly independent source excitation vectors. The source and sensor vectors produced during different excitation states are denoted by an attached parenthesized *excitation-state symbol*. The three source excitation vectors used in this analysis correspond to the source axes, hence

$$\boldsymbol{f}_1(S1) = \begin{bmatrix} 1 \\ 0 \\ 0 \end{bmatrix} \quad \boldsymbol{f}_1(S2) = \begin{bmatrix} 0 \\ 1 \\ 0 \end{bmatrix} \quad \text{and} \quad \boldsymbol{f}_1(S3) = \begin{bmatrix} 0 \\ 0 \\ 1 \end{bmatrix} \tag{7}$$

the set of two or three of these excitation vectors constitutes an *excitation pattern*. The corresponding sensor outputs are similarly denoted by $\boldsymbol{f}_5(S1)$, $\boldsymbol{f}_5(S2)$, and $\boldsymbol{f}_5(S3)$, respectively. Operation with other sets of excitation states is readily reduced to operation with this set of basis vectors. Note that the measurement matrix $\boldsymbol{R}$ is produced by assembling the sensor output vectors corresponding to excitation by the basis vectors in (7).

III. Position Determination

Three-axis sensing determines the complete signal vector produced at the sensor location by each excitation vector. Since the sensor orientation is unknown initially, position is determined from signal parameters that are unaffected by sensor orientation. This conveniently separates the position and orientation unknowns and therefore simplifies the system of trigonometric equations.

Orientation-Invariant Parameters

The field vectors produced at the sensor location (equivalently, the output vectors of a zero-orientation sensor) are transformed into the outputs of the true sensor by a sequence of orthogonal rotations, which preserve vector length and relative angle. Solutions for the unknown position of the sensor are therefore formulated in terms of squared magnitudes and the dot products of sensor output vectors, both of which are invariant under sensor orientation.

Since orthogonal rotations do not affect vector magnitudes and dot products, determination of those parameters can be simplified by omitting the $\boldsymbol{A}$ matrix from (4) and the rotations to the left of $\boldsymbol{S}$ in (5). Therefore, the columns of

$$\boldsymbol{S}\boldsymbol{T}_\beta\boldsymbol{T}_\alpha = \begin{bmatrix} \cos\alpha\cos\beta & \sin\alpha\cos\beta & -\sin\beta \\ \frac{1}{2}\sin\alpha & -\frac{1}{2}\cos\alpha & 0 \\ -\frac{1}{2}\cos\alpha\sin\beta & -\frac{1}{2}\sin\alpha\sin\beta & -\frac{1}{2}\cos\beta \end{bmatrix} \tag{8}$$

represent a set of sensor output vectors in some coordinate frame.

Three-State Excitation

Consider the squared vector magnitude produced by Z-axis (state $S3$) excitation of the source; from the third column of (8),

$$P(S3) = \frac{C^2}{\rho^6}\left(\sin^2\beta + \frac{1}{4}\cos^2\beta\right). \tag{9}$$

Substitution of $\sin^2\beta = z^2/\rho^2$ and $\cos^2\beta = (x^2 + y^2)/\rho^2$ into

TABLE II
SIGNS OF DOT PRODUCTS

Quadrant	Position Coordinates					Dot Products		
	x	y	z	α	β	$v(S1,S2)$	$v(S2,S3)$	$v(S3,S1)$
1	+	+	-	$0^\circ \ldots 90^\circ$	$0^\circ \ldots +90^\circ$	+	-	-
2	-	+	-	$90^\circ \ldots 180^\circ$	$0^\circ \ldots +90^\circ$	-	-	+
3	-	-	-	$-90^\circ \ldots -180^\circ$	$0^\circ \ldots +90^\circ$	+	+	+
4	+	-	-	$0^\circ \ldots -90^\circ$	$0^\circ \ldots +90^\circ$	-	+	-
5	+	+	+	$0^\circ \ldots 90^\circ$	$0^\circ \ldots -90^\circ$	+	+	+
6	-	+	+	$90^\circ \ldots 180^\circ$	$0^\circ \ldots -90^\circ$	-	+	-
7	-	-	+	$-90^\circ \ldots -180^\circ$	$0^\circ \ldots -90^\circ$	+	-	-
8	+	-	+	$0^\circ \ldots -90^\circ$	$0^\circ \ldots -90^\circ$	-	-	+

(9) then produces

$$P(S3) = \frac{C^2}{\rho^8}\left(\frac{1}{4}x^2 + \frac{1}{4}y^2 + z^2\right). \tag{10}$$

Application of geometric analogies and the normalizations $X = Cx/\rho^4$, $Y = Cy/\rho^4$, and $Z = Cz/\rho^4$ to (10) products a system of three linear equations

$$P(S1) = X^2 + \tfrac{1}{4}Y^2 + \tfrac{1}{4}Z^2 \tag{11}$$

$$P(S2) = \tfrac{1}{4}X^2 + Y^2 + \tfrac{1}{4}Z^2 \tag{12}$$

$$P(S3) = \tfrac{1}{4}X^2 + \tfrac{1}{4}Y^2 + Z^2. \tag{13}$$

Estimates of the squared, normalized position coordinates are given by

$$\begin{bmatrix}\hat{X}^2\\ \hat{Y}^2\\ \hat{Z}^2\end{bmatrix} = \frac{2}{9}\begin{bmatrix}5 & -1 & -1\\ -1 & 5 & -1\\ -1 & -1 & 5\end{bmatrix}\begin{bmatrix}P(S1)\\ P(S2)\\ P(S3)\end{bmatrix}. \tag{14}$$

Ambiguous position angles ($\hat{\alpha}$ and $\hat{\beta}$) can be determined directly from $|\hat{X}|$, $|\hat{Y}|$, and $|\hat{Z}|$ without denormalization. If C is known, the range estimate $\hat{\rho}$ is readily determined, since

$$\frac{C^2}{\rho^6} = X^2 + Y^2 + Z^2 = \frac{3}{2}\left[P(S1) + P(S2) + P(S3)\right]. \tag{15}$$

Once $\hat{\rho}$ has been determined, $|\hat{x}|$, $|\hat{y}|$, and $|\hat{z}|$ are obtained by denormalization.

Ambiguity Resolution

Quadrant ambiguity resolution is accomplished using the signs (polarities) of the dot products of the sensor output vectors. The three different dot products corresponding to the three excitation states of (7) are from (8)

$$v(S1,S2) = \frac{C^2}{\rho^6}\left(\frac{3}{8}\sin 2\alpha\right)(\cos^2\beta) \tag{16}$$

$$v(S2,S3) = \frac{C^2}{\rho^6}\left(-\frac{3}{8}\sin\alpha\right)(\sin 2\beta) \tag{17}$$

and

$$v(S3,S1) = \frac{C^2}{\rho^6}\left(-\frac{3}{8}\cos\alpha\right)(\sin 2\beta). \tag{18}$$

Inspection of Table II shows that any two of the three dot products removes two of the three quadrant ambiguities. The third dot product is redundant, and the remaining single-quadrant ambiguity (e.g., $(\hat{x},\hat{y},|\hat{z}|)$) is inherent in the field structure. It may, however, be resolved by either physical restrictions on position (e.g., $z < 0$) or orientation (e.g., $-90^\circ \leqslant \phi \leqslant +90^\circ$). If an orientation restriction is used, choice of the wrong candidate position is detected by an orientation estimate in an unallowed quadrant. If the sensor is located on the X_1, Y_1, or Z_1 axis, all three dot products are zero and therefore provide no ambiguity resolution information.

Two-State Excitation

The ambiguous position of a three-axis sensor with respect to a two-axis source can be determined from the two squared magnitudes and the dot product of the sensor output vectors. Since only one dot product is available, only one of the three quadrant ambiguities can be resolved from the information in the received signals (Table II).

Suppose that the source has only X and Y axes. The squared vector magnitudes are then $P(S1)$ and $P(S2)$, and are given by (11) and (12). The dot product $v(S1,S2)$ given by (16) is converted to normalized rectangular coordinates, thus

$$\begin{aligned} v(S1,S2) &= \frac{3}{4}\frac{C^2}{\rho^6}\cos\alpha\sin\alpha\cos^2\beta \\ &= \frac{3}{4}\frac{C^2}{\rho^6}\left(\frac{x}{\sqrt{x^2+y^2}}\right)\left(\frac{y}{\sqrt{x^2+y^2}}\right) \\ &\quad\cdot\left(\frac{x^2+y^2}{\rho^2}\right) = \frac{3}{4}XY. \end{aligned} \tag{19}$$

Subtraction of (12) from (11) eliminates unknown Z, hence

$$P(S1) - P(S2) = \tfrac{3}{4}(X^2 - Y^2). \tag{20}$$

Rearrangement of (19) gives unknown Y as a function of un-

known X (provided $X \neq 0$)

$$Y = \frac{4}{3} \frac{v(S1, S2)}{X}. \tag{21}$$

Substitution of (21) into (20) and rearrangement yields

$$X^4 - \{\tfrac{4}{3}[P(S1) - P(S2)]\} X^2 - \tfrac{16}{9} v^2(S1, S2) = 0. \tag{22}$$

The estimate $\hat{X}^2$ is found by solving (22) with the quadratic formula; the negative candidate for X^2 is discarded. Substitution of $|\hat{X}|$ into (21) produces $|\hat{Y}|$, and substitution of $|\hat{X}|$ and $|\hat{Y}|$ into either (11), or (12) produces $|\hat{Z}|$. Range $\hat{\rho}$ is then determined from (15) and used to denormalize the estimated position coordinates.

Better performance in the presence of noise can generally be obtained by using the sum of (11) and (12), thus

$$\hat{Z}^2 = 2[P(S1) + P(S2) - \tfrac{5}{4}(\hat{X}^2 + \hat{Y}^2)]. \tag{23}$$

If $v(S1, S2) = 0$, then either $X = 0$ or $Y = 0$. If $P(S1) - P(S2) > 0$, then $Y = 0$ and (20) determines $\hat{X}^2$; otherwise $X = 0$ and (20) determines $\hat{Y}^2$. In either special case, $\hat{Z}^2$ can be determined from (23).

Reciprocity requires that sensor-to-source coupling be the same as source-to-sensor coupling. The position of a two-axis sensor relative to a three-axis source can therefore be determined by forming vectors of the responses of each sensor axis to the three source axes. When these are used in place of the sensor output vectors in the preceding equations, the location of the three-axis source with respect to the sensor will be determined. After orientation has been determined, these position coordinates can be converted to source-frame coordinates.

IV. Orientation Determination

Sensor orientation can be determined from any two sensor output vectors that are not colinear.

Sensor Response

The orientation rotations (4) that convert the output of an equivalent zero-orientation sensor into the output of the true sensor can be expanded (by using Table I) to produce

$$\boldsymbol{A} = \begin{bmatrix} \cos\theta\cos\psi & \cos\theta\sin\psi & -\sin\theta \\ -\cos\phi\sin\psi & \cos\phi\cos\psi & \\ +\sin\phi\sin\theta\cos\psi & +\sin\phi\sin\theta\sin\psi & \sin\phi\cos\theta \\ \sin\phi\sin\psi & -\sin\phi\cos\psi & -\cos\phi\cos\theta \\ +\cos\phi\sin\theta\cos\psi & +\cos\phi\sin\theta\sin\psi & \end{bmatrix}. \tag{24}$$

The elements of $\boldsymbol{A}$ represent the sensor response to unit-amplitude fields aligned with the source axes.

It is apparent that estimates of the orientation angles can be made from an estimate $\hat{\boldsymbol{A}}$ of the orientation matrix. Multiplicative errors common to all elements (produced by errors in the range estimate, magnetic moment, or sensor gain) are eliminated by using *ratios* of the elements of $\hat{\boldsymbol{A}}$, thus

$$\hat{\psi} = \arctan \frac{\hat{a}_{12}}{\hat{a}_{11}} \tag{25}$$

and

$$\hat{\phi} = \arctan \frac{\hat{a}_{23}}{\hat{a}_{33}}. \tag{26}$$

(Note that a four-quadrant inverse tangent will place $\hat{\psi}$ and $\hat{\phi}$ in the proper quadrant.) Elevation $\hat{\theta}$ can be determined from

$$\hat{\theta} = \arctan \frac{\hat{a}_{13}}{\hat{a}_{11}/\cos\hat{\psi}} \tag{27}$$

or three similar ratios using $\hat{a}_{13}, \hat{a}_{12}, \hat{a}_{23}$, and $\hat{a}_{33}$. Orientation angles can generally be determined from any two rows or columns of $\hat{\boldsymbol{A}}$ by the use of more complicated trigonometic relationships.

Three-State Excitation

Since the set of three sensor output vectors spans three-dimensional space, it is evident from (3) that $\hat{\boldsymbol{A}}$ can be obtained from the measurement matrix $\hat{\boldsymbol{A}}$ by

$$\hat{\boldsymbol{A}} = \frac{\hat{\rho}^3}{C} \hat{\boldsymbol{R}} \hat{\boldsymbol{Q}}^{-1}. \tag{28}$$

The inverse-coupling matrix $\hat{\boldsymbol{Q}}^{-1}$ is computed using estimated values $\hat{\alpha}$ and $\hat{\beta}$. Note that actual matrix inversion is unnecessary, since

$$\boldsymbol{Q}^{-1} = (\boldsymbol{T}_{-\alpha}\boldsymbol{T}_{-\beta}\boldsymbol{S}\boldsymbol{T}_{\beta}\boldsymbol{T}_{\alpha})^{-1} = \boldsymbol{T}_{-\alpha}\boldsymbol{T}_{-\beta}\boldsymbol{S}^{-1}\boldsymbol{T}_{\beta}\boldsymbol{T}_{\alpha} \tag{29}$$

where

$$\boldsymbol{S}^{-1} = \begin{bmatrix} 1 & 0 & 0 \\ 0 & -2 & 0 \\ 0 & 0 & -2 \end{bmatrix}. \tag{30}$$

Two-State Excitation

In a two-state system, the measurement matrix has only two nonzero columns. Consequently, postmultiplication of $\hat{R}$ by the inverse field-coupling matrix as in (28) does not produce $\hat{\boldsymbol{A}}$.

The cross product of two vectors is orthogonal to the two vectors; the set of two noncolinear vectors and their cross product therefore spans three-dimensional space. Since the orthogonal rotations in $\boldsymbol{A}$ that convert $\boldsymbol{Q}$ into $\boldsymbol{R}$ preserve the angles between vectors, cross-product vectors can be used in place of the "missing" vectors for the third excitation state.

The synthetic 3 X 3 measurement matrix has the form

$$\boldsymbol{R}' = [\boldsymbol{f}_S(S1) \mid \boldsymbol{f}_S(S2) \mid \boldsymbol{f}_S(CP)] \tag{31}$$

where

$$\boldsymbol{f}_S(CP) = \boldsymbol{f}_S(S1) \times \boldsymbol{f}_S(S2). \tag{32}$$

Similarly, the third column of the computed field-coupling matrix $\hat{\boldsymbol{Q}}$ is replaced with the cross product of the first two columns, producing matrix $\hat{\boldsymbol{Q}}'$. The estimated orientation

matrix is then given by

$$\hat{\boldsymbol{A}} = \frac{\hat{\rho}^3}{C}\,\hat{\boldsymbol{R}}'\,(\hat{\boldsymbol{Q}}')^{-1}. \tag{33}$$

For computational convenience, it may be desirable to multiply the elements of $\hat{\boldsymbol{R}}$ and $\hat{\boldsymbol{Q}}$ by $\hat{\rho}^3/C$ before computing the cross products; this results in the cross-product vectors and sensor output vectors of roughly the same magnitude.

Matrix inversion can be avoided by an alternative method of determining orientation. Linear combinations of the two field vectors at the sensor location form two orthogonal synthetic field vectors; the same combinations of two sensor output vectors produce the analogous synthetic response vectors. The two synthetic output vectors are regarded as two columns of an orientation matrix, allowing determination of orientation angles with respect to the synthetic field vectors. These angles are then converted to orientation angles defined with respect to the source coordinate frame.

V. Sensitivity

The sensitivity of the position and orientation estimates to errors in the measurements can be determined from a system of partial derivatives. However, such an analysis is quite tedious unless it is accomplished by numerical techniques. The subsequent discussion derives some simple limits on estimation errors for three-state excitation; limits applicable to two-state excitation can be inferred by comparisons of the simulations in the next section. These limits may be used for preliminary design calculations and illustrate the behavior of the errors as functions of the position and orientation of the sensor.

Position Errors

Consider the total absolute position coordinate error

$$\epsilon = |\Delta x| + |\Delta y| + |\Delta z| \tag{34}$$

where each estimated coordinate has the form

$$\hat{x} = x + \Delta x = \sqrt{x^2 + \Delta(x^2)} \simeq \begin{cases} x + \dfrac{1}{2x}\,\Delta(x^2), & x \not\simeq 0 \\ \sqrt{\Delta(x^2)}, & x \simeq 0. \end{cases} \tag{35}$$

Use of the Schwartz inequality and the normalization $\hat{x}^2 = \rho^8 \hat{X}^2/C^2$ produces

$$|\Delta(x^2)| \leqslant \frac{\rho^8}{C^2}\,|\Delta(X^2)| + \frac{X^2}{C^2}\,|\Delta(\rho^8)|. \tag{36}$$

Manipulation of (15) then produces

$$\Delta(\rho^8) = -\frac{8}{9}\,\rho^2\,\frac{C^2}{P(T)}\,\frac{\Delta P(T)}{P(T)} \tag{37}$$

where $P(T) = P(S1) + P(S2) + P(S3)$ and $\Delta P(T) = \Delta P(S1) + \Delta P(S2) + \Delta P(S3)$.

A simple form for ϵ can be obtained when $|x| = |y| = |z| = \rho/3^{1/2}$. The errors ΔX^2, ΔY^2, and ΔZ^2 are related to the measurement errors $\Delta P(S1)$, $\Delta P(S2)$, and $\Delta P(S3)$ by (14), and (15) is used to simplify the sum $X^2 + Y^2 + Z^2$. The Schwartz inequality is again used to obtain the worst-case limit

$$\epsilon_{\max} = \frac{32\ 3^{1/2}}{27}\,\frac{\Delta P(T)}{P(T)}\,\rho \simeq 2.053\,\frac{\Delta P(T)}{P(T)}\,\rho. \tag{38}$$

The factor $1/x$ in (35) and the analogous forms for $y + \Delta y$ and $z + \Delta z$ cause the error sensitivity to increase as the position coordinates differ from $|x| = |y| = |z| = \rho/3^{1/2}$. It is also evident that position error can be greatly increased when the sensor is located on a coordinate axis; for example, $1.01^{1/2} \simeq 1.005$ while $0.01^{1/2} = 0.1$, indicating errors differ by a factor of 50. When the initial position estimate indicates that an unsatisfactory degradation of accuracy is possible, be the measurements should be mathematically rotated away from the axes. The position is then estimated with respect to the rotated coordinate frame and transformed back to the source coordinate frame.

Orientation Errors

Orientation angles are estimated by inverse tangents of the ratios of two elements of the estimated orientation matrix $\hat{\boldsymbol{A}}$. Errors in the estimated angles can therefore readily be related to errors in estimating the elements of $\hat{\boldsymbol{A}}$. For example, a small-angle expansion of (25) produces

$$\Delta\psi = \frac{\cos\psi}{\cos\theta}\,\Delta a_{12} - \frac{\sin\psi}{\cos\theta}\,\Delta a_{11}. \tag{39}$$

The unbounded increase in the errors for $\theta \simeq \pm 90^\circ$ can be avoided by recomputing the estimated angles using inverse cotangents of the inverse ratios whenever the estimated elevation produces $|\cos\theta| < \frac{1}{2}$; the "damage" done by division by $\cos\theta$ in (39) is therefore limited to a factor of 2. If Δa represents the maximum error occurring in an individual element of $\hat{\boldsymbol{A}}$, the Schwartz inequality applied to (39) produces

$$|\Delta\psi| \leqslant 2\sqrt{2}\,|\Delta a| \simeq 2.828\,|\Delta a|. \tag{40}$$

The errors in the elements of $\hat{\boldsymbol{A}}$ arise from two sources. Errors in the measurements $\hat{\boldsymbol{R}}$ caused by atmospheric noise or scattering by the conducting ground are converted directly into errors Δa_{ij} by the transformation given in (29). Since the orthogonal rotations do not alter the magnitudes of the errors, the worst case effect is multiplication by a factor of 2 caused by elements of $\boldsymbol{S}^{-1}$. Errors in the estimated position azimuth and elevation ($\hat{\alpha}$ and $\hat{\beta}$) produce imperfect cancellation of the position (i.e., $\boldsymbol{Q}\hat{\boldsymbol{Q}}^{-1} \neq I$). The contributions to an error Δa caused by these errors cannot exceed $2\,|\Delta\alpha|$ or $2\,|\Delta\beta|$.

VI. System Design

The two most significant considerations in the design of a quasi-static-field position-finding system are 1) determination of the maximum allowable excitation frequency for specified maximum measurement errors due to ground conductivity, and 2) determination of a transmitter magnetic moment that ensures no more than a specified rms measurement error due to atmospheric (or other) noise. Design guidelines and simulated performance are subsequently presented.

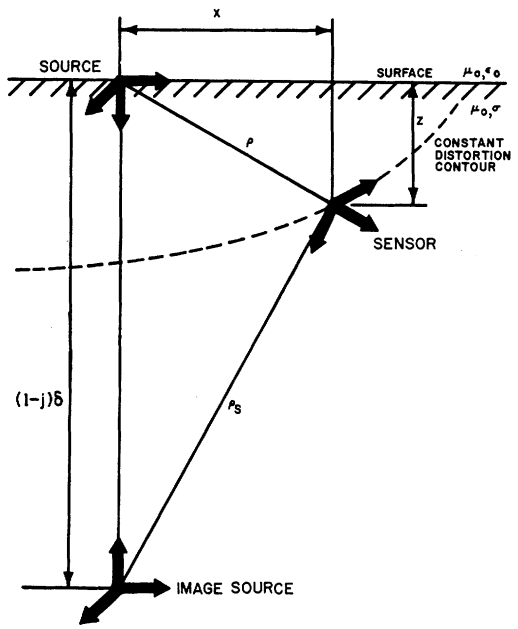

Fig. 4. Model for complex-image theory.

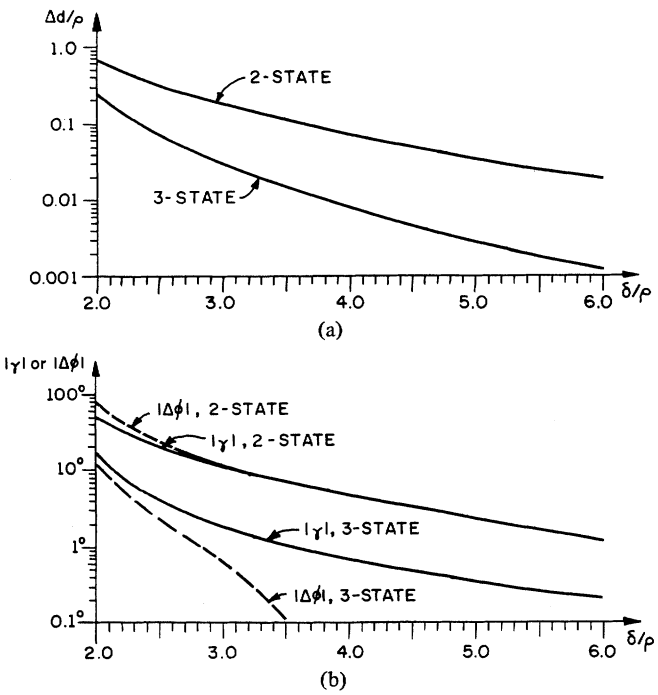

Fig. 5. Simulated performance in a conducting ground; sensor is located at $(x, y, z) = (1, 1, 1)$. (a) Normalized position error. (b) Orientation line-of-sight error γ and roll error $\Delta\phi$.

Frequency Selection

Deviations form free-space quasi-static field geometry caused by the conducting ground produce errors in the position and orientation measurements. Since the maximum allowable measurement errors can be presumed to be small, the maximum allowable deviation of field geometry can similarly be presumed to be small. Consequently, exact characterization of the subsurface fields through numerical integration can be avoided by the use of complex-image theory.

Complex-image theory [11]-[13] has been applied to many problems involving quasi-static fields and a conducting half space. In many above-surface applications, complex-image theory predicts the fields very accurately (within 10 percent). In this application, it provides an accurate first-order approximation to the initial deviation of the actual subsurface fields from free-space characteristics as depth is increased. Because it requires only complex arithmetic it is much easier to use and consumes much less computation time than does an exact field calculation.

Assume that the source is located on the surface of a uniformly conducting half space, as shown in Fig. 4. Complex-image theory replaces the ground with an image located at a depth $d = (1 - j)\,\delta$, where δ is the electrical skin depth given by

$$\delta = \left(\frac{2}{\omega\mu_0\sigma}\right)^{1/2} \tag{41}$$

$\mu_0 \simeq 4\pi \cdot 10^{-7}$ is the permeability of free space, and σ is the conductivity of the ground. The source X-axis and Y-axis (horizontal) dipoles of the image source have the same orientations as those in the true source, while Z-axis (vertical) dipole of the image source is opposite in orientation to that in the true source. Primary (true-source) and secondary (image-source) fields at the sensor location are then calculated and added.

The relative amplitudes of the primary and secondary fields are then proportional to $1/\rho^3$ and $1/\rho_s^3$, respectively. It is evident from Fig. 4 that for given distance ρ, the greatest effect of the ground occurs when the sensor is located directly below the source. If the worst-case conditions of orientation and phase alignment of the primary and secondary field vectors are assumed, then

$$\frac{\Delta P}{P} = \frac{2f\Delta f}{f^2} = 2\frac{\Delta f}{f} = 2\frac{\rho_s^3}{\rho_s^3} \tag{42}$$

where f represents a field-amplitude measurement.

Equation (42) can now be used to constrain position and orientation errors; for example, combination with (38) yields the design requirement

$$\frac{\rho}{\rho_s} \leqslant 0.624 \sqrt[3]{\frac{\epsilon_{\max}}{\rho}}. \tag{43}$$

If one requires that $\epsilon_{\max}/\rho < 0.01$, then $\rho/|\rho_s| < 0.135$. If the sensor is located directly below the source, $\rho + \rho_s = (1 - j)\,\delta$, hence $\rho + |\rho_s| \geqslant \sqrt{2\delta}$ and $\delta \geqslant 5.94\,\rho$. Operation at a depth of 300 m then requires $\delta \geqslant 1.783$ km; if $\sigma = 0.01$ mho/m, the maximum usable frequency is 7.9 Hz.

Simulated performance in the presense of conducting ground is shown in Fig. 5. The parameters graphed are position error $\Delta d = [(\Delta x)^2 + (\Delta y)^2 + (\Delta z)^2]^{1/2}$ and orientation line-of-sight error $|\gamma|$ and roll error $|\Delta\phi|$. On the basis of these simulations, it appears that two-state operation requires a skin depth 1.5 to 2 times that required for three-state operation with the same errors. Equivalently, a transmission frequency lower than that for three-state operation by a factor of 0.44 to 0.25 is required.

Noise and Transmitter Magnetic Moment

Once an operating frequency has been selected, the expected electrical noise level can be determined from published data [14]. The noise level can then be converted into a required carrier-to-carrier ratio and subsequently into a required transmitter magnetic moment for a given position or orientation accuracy. Since the effects of the conducting ground are assumed to be relatively small, the expected value of the subsurface atmospheric noise is essentially the same as the on the surface.

The sum of the errors in the squared vector magnitudes is approximately

$$\Delta P(T) = 2\,|\boldsymbol{f}_5(S1)|\,\Delta|\boldsymbol{f}_5(S1)| + 2\,|\boldsymbol{f}_5(S2)|\,\Delta|\boldsymbol{f}_5(S2)| + 2\,|\boldsymbol{f}_5(S3)|\,\Delta|\boldsymbol{f}_5(S3)|. \quad (44)$$

If the noise errors are small in comparison to the signal amplitudes, the effects of noise vectors that are in phase quadrature to the signal vectors are negligible. If all three significant noise errors have the same expected rms value σ_n, the expected squared error in the sum of the squared vector magnitudes is

$$\mathrm{E}\,[|\Delta P(T)|^2] = 4\,[|\boldsymbol{f}_5(S1)|^2 + |\boldsymbol{f}_5(S2)|^2 + |\boldsymbol{f}_5(S3)|^2]\,\sigma_n^2 = 4P(T)\,\sigma_n^2. \quad (45)$$

While the above expression can be used to constrain the position of orientation errors or to determine a required $P(T)$, it does not yield a simple relationship when combined with (38) or (40). It is therefore more convenient to use the simulated performance data presented in Fig. 6; each point represents the rms average of errors in 10 estimates.

Since the signal and noise amplitudes vary from state to state and axis to axis, the carrier-to-noise ratio (CNR) is arbitrarily defined as total (three states) signal power divided by total (three states, three axes) noise power. If the rms noise is expected to be the same for all three axes and all three excitation states, this produces

$$\mathrm{CNR} = \frac{\frac{1}{2}P(T)}{9\sigma_n^2} = \frac{C^2}{27\rho^6\sigma_n^2}. \quad (46)$$

Although the third state is not actually excited, (46) is used without modification for two-state operation.

To illustrate the use of the above relationships, suppose that an rms position error of 0.01 ρ is required at a distance of 300 meters through ground of conductivity $\sigma = 0.01$ mho/m. For three-state operation, Fig. 6 specifies CNR $\geqslant$ 32 dB = 1584. Electric-field rms atmospheric noise measured in a 1-Hz bandwidth is expected [14] to be in the range of -72 dB relative to 1 V/m. A 20-dB effective noise power reduction can be obtained by integrating each signal for 100 s. This produces an effective noise level of -92 dB relative to 1 V/m or 25.1 μV rms, which is equivalent to a magnetic-field noise of 0.067 μA/m rms. Substitution of σ_n, ρ^6, and CNR into (46) yields $C = 372$, hence $M = NIA = 2\pi C = 2338$.

This can be achieved by square loops of $N = 40$ turns with 3-m sides driven by $I_{\mathrm{rms}} = 6.49\ \mathrm{A_{rms}}$. The use of #12 aluminum wire produces loop with weights of 4.29 kg (each) and resistances of 3.8 Ω. The required 160-W driving power can be provided by a number of commercially available audio power amplifiers; current monitoring should be used to maintain exactly the desired magnetic moment. The inductance of such loops is approximately 28.6 mH; if the power amplifier cannot tolerate the resultant reactance (1.42 Ω at 7.9 Hz), it can be cancelled with a series-connected 14 200-μF capacitor.

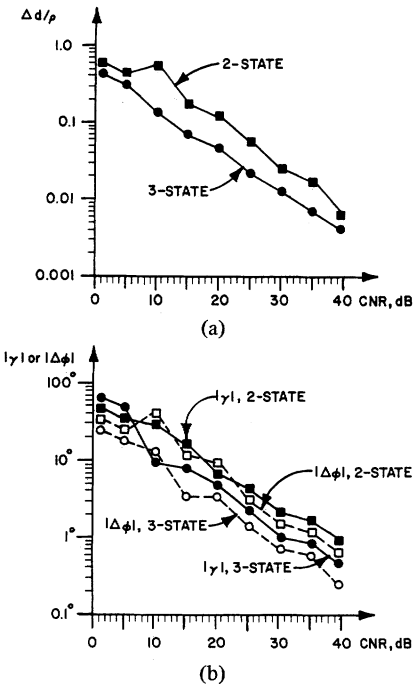

Fig. 6. Simulated performance in the presence of Gaussian noise; sensor is located at $(x, y, z) = (1, 1, 1)$. Plotted points represent rms averages of 10 trials. (a) Normalized position error. (b) Orientation line-of-sight error γ and roll error $\Delta\phi$.

Individual sensor outputs should be integrated to minimize the effects of noise; squared vector magnitudes and dot products should be computed only *after* signal integration is completed. Estimates of squared vector magnitudes are biased slightly larger than their true value, since the expected contribution of noise to the square of a noisy signal is always positive; i.e., $\mathrm{E}\,[(f+n)^2] + \mathrm{E}\,[f]^2 + \mathrm{E}\,[n^2]$. When the expected noise power is known *a priori* or is estimated by another receiver, it may be possible to improve the estimates of squared vector magnitudes by subtracting the estimated noise-power contributions. However, if the noise-power contributions are estimated by averaging the squares of the received signals, the errors in the noise-power estimates are comparable to the noise power and therefore are of little use. Since low-frequency atmospheric noise has an impulsive character, typical improvements of 10 to 15 dB can be obtained by clipping or editing the signals [15].

VII. Conclusions

This paper has described a position-and-orientation-measurement technique based upon multiaxis excitation and sensing of quasi-static magnetic fields. The effects of the conducting ground are overcome by using extremely low-frequency signals; the effects of high atmospheric noise levels are overcome by using long signal-integration time. Applications include subsurface drill guidance and the location of trapped mine

workers. System design can be accomplished using the equations and simulated performance data presented.

REFERENCES

[1] H. K. Sacks, "Trapped-miner location and communication systems," *Underground Mine Communications, Part 4, Section-to-Place Communications*, U.S. Bureau of Mines Information Circular 8745, 1977.

[2] R. G. Olsen and A. J. Farstad, "Electromagnetic direction finding experiments for location of trapped miners," *IEEE Trans. Geosci. Electron.*, vol. GE-11, pp. 178–185, Oct. 1973.

[3] J. Durkin, "Assessment of present techniques for the location of trapped miners," in *Proc. 5th WVU Conf. Coal Mine Electrotechnology* (Morgantown, WVA), pp. 1-1–1-16, July 30, Aug. 1, 1980.

[4] T. W. H. Caffey, "Locating a buried earth penetrator," Sandia Laboratories, Albuquerque, NM, Rep. SAND77-0646, Nov. 1977.

[5] —, "Locating a buried magnetic dipole," in *Proc. Electromagnetic Guided Waves Workshop* (Boulder, CO), Mar. 28–30, 1978.

[6] L. H. Rorden, T. C. Moore, E. C. Fraser, and L. R. Bulduc, "Phase 1—Development of a system concept for location of trapped miners in deep mines by an electromagnetic method," Develco, Inc., Sunnyvale, CA, Phase I Rep., Contract J0199009, Oct. 1979.

[7] F. H. Raab and P. K. Hansen, "Electromagnetic retransmission system for locating trapped mine workers," Polhemus Navigation Sciences, Inc., Essex Junction, VT; Final Rep. Contract H0188071, Feb. 1980.

[8] F. H. Raab, E. B. Blood, H. R. Jones, and T. O. Steiner, "Magnetic position and orientation tracking system," *IEEE Trans. Aerospace Electron. Syst.*, vol. AES-15, pp. 709–718, Sept. 1979.

[9] F. H. Raab, "Remote object position locater," U.S. Patent 4 054 881, Oct. 18, 1977.

[10] M. R. Kraichman, *Handbook of Electromagnetic Propagation in Conducting Media*, 2nd Ed., Headquarters Naval Material Command, Washington, DC, 1976 (USGPO stock no. 008-040-00074-5).

[11] J. T. Weaver, "Image theory for an arbitrary quasi-static field in the presence of a conducting half-space," *Radio Sci.*, vol. 6, pp. 647–653, 1971.

[12] P. R. Bannister and R. L. Dube, "Modified image theory quasi-static range subsurface-to-subsurface and subsurface-to-air propagation equations," Naval Underwater Systems Center, New London, CT, Tech. Rep. 5648.

[13] P. R. Bannister, "Summary of image theory expressions for the quasi-static field of antennas at or above the earth's surface," *Proc. IEEE*, vol. 67, pp. 1001–1008, July 1979.

[14] E. L. Maxwell, "Atmospheric noise from 20 Hz to 30 kHz," *Radio Sci.*, vol. 2, no. 6, pp. 637–644, June 1967.

[15] J. E. Evans and A. S. Griffiths, "Design of a Sanguine noise processor based upon world-wide extremely low frequency (ELF) recordings," *IEEE Trans. Commun.*, vol. COM-22, pp. 83–87, Jan. 1974.

*

Frederick H. Raab (S'66–M'72–SM'80) is a native of Waterloo, IA, and received the B.S., M.S., and Ph.D. degrees in electrical engineering from Iowa State University, Ames, in 1968, 1970, and 1972, respectively.

Since starting Green Mountain Radio Research Company, Burlington, VT, in 1980, he has been involved in special-purpose *RF* design projects and radio-navigation studies. From 1975 to 1980, he was with Polhemus Navigation Sciences, Inc., and was involved with terrestrial use of Loran-C, an electromagnetic subsurface location system, and other special-purpose position-finding systems. From 1971 to 1975, he was with Cincinnati Electronics Corporation and was involved with the design of high-efficiency power amplifiers and search-and-rescue navigation systems. He holds two patents and has authored or coauthored over thirty technical papers and one textbook, *Solid State Radio Engineering*. His professional interests include power amplifiers, *RF* design, communications, signal processing, and radio navigation.

Dr. Raab is a member of the Institute of Navigation, the International Omega Association, the Wild Goose Association, Eta Kappa Nu, and Sigma Xi.